# Ab initio simulation of the IR spectra of pyrope, grossular, and andradite. J Comput Chem

**ARTICLE** *in* JOURNAL OF COMPUTATIONAL CHEMISTRY · OCTOBER 2008

Impact Factor: 3.59 · DOI: 10.1002/jcc.20993 · Source: PubMed

# *Ab initio* Simulation of the IR Spectra of Pyrope, Grossular, and Andradite

**C. M. ZICOVICH-WILSON[1], F. J. TORRES,[1] F. PASCALE,[2] L. VALENZANO,[1] R. ORLANDO,[3] R. DOVESI[1]**

[1]*Dipartimento di Chimica IFM, Università di Torino and NIS-Nanostructured Interfaces and Surfaces - Centre of Excellence, Via P. Giuria 7, 10125 Torino, Italy*

*On sabbatical leave from: Facultad de Ciencias, Universidad Autónoma del Estado de Morelos, Av. Universidad, 1001, Col. Chamilpa, 62209 Cuernavaca (Morelos), Mexico*

[2]*Laboratoire de Cristallographie et Modélisation des Matériaux Minéraux et Biologiques, UMR-CNRS-7036, Université Henri Poincaré - Nancy I, B.P. 239, 54506 Vandœuvre-lès-Nancy Cedex 05, France*

[3]*Dipartimento di Scienze e Tecnologie Avanzate, Università del Piemonte Orientale, Via Bellini 25/G, 15100 Alessandria, Italy*

*Received 29 October 2007; Revised 29 February 2008; Accepted 2 March 2008*
*DOI 10.1002/jcc.20993*
*Published online 8 July 2008 in Wiley InterScience (www.interscience.wiley.com).*

**Abstract:** IR spectra of pyrope $Mg_3Al_2Si_3O_{12}$, grossular $Ca_3Al_2Si_3O_{12}$ and andradite $Ca_3Fe_2Si_3O_{12}$ garnets were simulated with the periodic *ab initio* CRYSTAL code by adopting an all-electron Gaussian-type basis set and the B3LYP Hamiltonian. Two sets of 17 $F_{1u}$ Transverse Optical (TO) and Longitudinal Optical (LO) frequencies were generated, together with their intensities. Because the generation of LO modes requires knowledge of the high frequency dielectric constant $\varepsilon^{\infty}$ and Born effective charges, they were preliminary evaluated by using a finite field saw-tooth model and well localized Wannier functions, respectively. As a by-product, the static dielectric constant $\varepsilon^{0}$ was also obtained. The agreement of the present calculated wavenumbers (i.e. peak positions) with the available experimental data is excellent, in that the mean absolute difference for the full set of data smaller than 8 $cm^{-1}$. Missing peaks in experimental spectra were found to correspond to modes with low calculated intensities. Correspondence between TO and LO modes was established on the basis of the overlap between the eigenvectors of the two sets and similarity of isotopic shifts; as result, the so called *LO-TO* splitting could be determined. Animation of the normal modes was employed to support the proposed pairing.

 J Comput Chem 29: 2268–2278, 2008

**Key words:** vibrational spectrum; dynamical matrix; periodic calculations; ab initio; Gaussian basis sets

## Introduction

Garnets $X_3^{II}Y_2^{III}Si_3O_{12}$ are important rock-forming silicates, as major constituents of the Earth's upper mantle and relevant phases of high-pressure metamorphic rocks in the Earth's crust.[1] It was recognized that garnets represent excellent reference systems for the study of the vibrational spectroscopic properties of silicates despite their relatively complex structure and large unit cell. Because of their high symmetry (space group $Ia\bar{3}d$) garnets present a relatively simple vibrational spectrum (17 IR and 25 Raman active modes). Additionally, the large variety of compositionally end-members, permits one to follow changes in the spectra with changing chemistry and to infer thermodynamic properties.[2,3]

In two previous articles, the Transverse Optical IR-active modes as well as the Raman-active modes of pyrope[4] and andradite[5] were calculated and compared with experimental data.[3,6,7] Moreover, the effect of the basis set size and some computational parameters were discussed into detail. In the present article we extend these studies in various directions: first, we include grossular in the set of systems investigated. Second, we evaluate Longitudinal Optical (LO) modes, that were not included in our previous investigations because, at the time, we were unable to compute the high frequency dielectric constant ($\varepsilon^{\infty}$) and Born charges ($Z^*_{\alpha}$), which are components of

***Correspondence to:*** R. Dovesi; e-mail: roberto.dovesi@unito.it

Contract/grant sponsor: MURST; contract/grant number: 25982-002

Contract/grant sponsor: Regione Piemonte, Institute for Scientific Interchange - CRT foundation, University of Turin

Contract/grant sponsor: CONACYT; contract/grant number: 8EPO5-46983

the correction to the dynamical matrix necessary to obtain the LO modes (see next section). $\varepsilon^0$ is obtainable from $\varepsilon^\infty$, and both $\varepsilon^0$ and $\varepsilon^\infty$ for the three systems (pyrope, andradite, and grossular) are compared to experimental data. Finally, the problem of the possible one-to-one LO-TO pairing for the various modes is tackled by using various tools, including overlap between TO and LO eigenvectors, isotopic substitution, and animation of the modes. The availability of excellent experimental TO and LO infrared data[3,8–10] for the three systems allows a very careful comparison with our simulated data and shows that calculation and experiment can be considered complementary tools.

To the authors' knowledge, this is the first *ab initio* investigation of the TO and LO IR modes of a garnet compound.

## Computational Details: Models and Methods, Basis Set and Geometry

Because the majority of the experimental data are collected on natural samples that are almost pure pyrope, grossular, and andradite, structures with end-member composition were considered for the construction of the models employed in our simulations. All the quantum-mechanical calculations have been performed with the CRYSTAL06 program[11] and, as in our previous works on garnets,[4,5] the B3LYP Hamiltonian[12] has been employed. It contains a hybrid HF/DF exchange correlation term and is widely and successfully used in molecular quantum chemistry[13] as well as in solid state calculations, where it has been shown to reproduce equilibrium geometries and vibrational frequencies[4,5,14–16] in excellent agreement with experimental data.[14,17] Computational conditions (tolerances for the truncation of the infinite Coulomb and exchange sums, SCF convergence criteria, grid size for integration of the DFT exchange and correlation contribution, and number of points in the reciprocal space) were set at the same values as in our previous studies of pyrope[4] and andradite,[5] where the effect of the basis set size on the calculated geometries and frequencies was documented. Here, basis set B (BSB) of ref. 4 was used for pyrope. It contains 8-511G(1), 8-6311(1) and 8-411G(1) contractions for Mg, Si, and O atoms, respectively. For Al, a slightly improved 8-611G(1) contraction was adopted, which provides essentially the same frequencies as the one used in ref. 4. The same Si and O basis sets have been used also for the other systems (see below for oxygen). For andradite, BSC of ref. 5 was adopted, which defines 8-6411G(3) and 8-64111G(41) contractions for Ca and Fe. In the latter notation, *d* function contractions are given in parentheses: (41) means that there are 2 d shells; the first contains a 4-G contraction, the second a single Gaussian. The exponents ($\zeta_{sp}$ in bohr$^{-2}$ units) of the most diffuse *sp* shells are: 0.22 (Mg), 0.28 (Ca), 0.35 (Al), 0.25 (Fe), 0.13 (Si), 0.20 (O for andradite), and 0.25 (for pyrope and grossular). The exponents ($\zeta_d$ in bohr$^{-2}$ units) of the most diffuse *d* shells are: 0.50 (Mg), 0.38 (Ca), 0.50 (Al), 0.43 (Fe), 0.60 (Si), and 0.5 (O). The basis sets are available at the CRYSTAL website.[18]

Structures were optimized by using the analytical first derivatives of the energy with respect to the atomic fractional coordinates and cell parameters. The highly symmetric garnet structure (space group $Ia\bar{3}d$) contains 48 point-symmetry operators and belongs to the $O_h$ point group. The general chemical formula of garnets is: $X_3^{II}Y_2^{III}Si_3O_{12}$, where X, Y, and the Si atoms are in dodecahedral ($D_2$), octahedral ($S_6$), and tetrahedral ($S_4$) special positions, respectively, whereas the oxygen atom is in a general position with $x \approx 0.04$, $y \approx 0.05$, and $z \approx 0.65$ (in fractional coordinates) according to X-ray diffraction studies performed for different end-member silicate garnets.[19–21] Table 1 documents the good agreement between calculated and experimental geometries for the three compounds. For example, the lattice parameter is overestimated by about 1%, and the Y–O and Si–O distances by 0.01 − 0.02 Å, with a maximum of 0.03 Å for Fe–O (from 2.050 to 2.019 Å).

**Table 1.** Calculated and Experimental Geometry of Pyrope, Grossular, and Andradite.

| | Pyrope | | Grossular | | Andradite | |
|---|---|---|---|---|---|---|
| | Calc | Exp[a] | Calc | Exp[b] | Calc | Exp[c] |
| *a* | 11.5447 | 11.4390 | 11.9368 | 11.8450 | 12.1960 | 12.0510 |
| $O_x$ | 0.03214 | 0.03291 | 0.03740 | 0.03823 | 0.03893 | 0.03914 |
| $O_y$ | 0.04971 | 0.05069 | 0.04515 | 0.04528 | 0.04838 | 0.04895 |
| $O_z$ | 0.65344 | 0.65331 | 0.65156 | 0.65137 | 0.65617 | 0.65534 |
| $X_1O$ | 2.2052 | 2.1959 | 2.3301 | 2.3218 | 2.3780 | 2.3584 |
| $X_2O$ | 2.3648 | 2.3335 | 2.5058 | 2.4865 | 2.5331 | 2.4953 |
| YO | 1.8987 | 1.8850 | 1.9398 | 1.9255 | 2.0497 | 2.0186 |
| SiO | 1.6496 | 1.6337 | 1.6627 | 1.6459 | 1.6612 | 1.6492 |

*a* is the lattice parameter (Å), $O_i$ are the oxygen fractional coordinates. $X_1O$, $X_2O$, YO, SiO are atom-atom distances (Å). X is Mg for pyrope, and Ca for grossular and andradite, whereas Y is Al for pyrope and grossular and Fe for andradite.
[a]Ref. 19.
[b]Ref. 20.
[c]Ref. 21.

## The Dynamical Matrix

The behavior of the phonons with wave vector **k** close to the center of the Brillouin zone can be well described by adopting the dipole approach, according to which only center-zone phonons ($\mathbf{k} = \mathbf{0}$) are considered and the dependence on the direction of **k**, resulting from the long-range nature of the electrostatic field in polar materials, is taken into account by considering the limiting cases $\mathbf{k} \to \mathbf{0}$.

The Dynamical Matrix (DM) can be expressed as the sum of two terms

$$W_{\alpha i,\beta j}(\mathbf{k} \to \mathbf{0}) = W_{\alpha i,\beta j}(\mathbf{k} = \mathbf{0}) + W^{\mathrm{NA}}_{\alpha i,\beta j}(\mathbf{k} \to \mathbf{0}), \qquad (1)$$

where greek and latin indices run over the atoms in the primitive cell and the three directions in the cartesian space, respectively.

### *The Analytical Part of the Dynamical Matrix*

The analytical part of DM is given by

$$W_{\alpha i,\beta j}(\mathbf{k} = \mathbf{0}) = \frac{1}{\sqrt{M_\alpha M_\beta}} H_{\alpha i,\beta j} \qquad (2)$$

**Table 2.** Atomic Born Effective Charge Tensors for the Elements of Pyrope, Grossular, and Andradite.

| | X | Y | Si | O |
|---|---|---|---|---|
| Py. | $\begin{pmatrix} 2.42 & 0.00 & 0.00 \\ 0.00 & 2.20 & 0.22 \\ 0.00 & 0.22 & 2.20 \end{pmatrix}$ | $\begin{pmatrix} 3.14 & -0.23 & -0.15 \\ -0.15 & 3.14 & -0.23 \\ -0.23 & -0.15 & 3.14 \end{pmatrix}$ | $\begin{pmatrix} 3.23 & 0.00 & 0.00 \\ 0.00 & 3.05 & -0.08 \\ 0.00 & 0.08 & 3.05 \end{pmatrix}$ | $\begin{pmatrix} -1.80 & 0.06 & -0.32 \\ 0.12 & -1.65 & 0.09 \\ -0.37 & 0.12 & -2.16 \end{pmatrix}$ |
| Gr. | $\begin{pmatrix} 2.63 & 0.00 & 0.00 \\ 0.00 & 2.22 & 0.19 \\ 0.00 & 0.19 & 2.22 \end{pmatrix}$ | $\begin{pmatrix} 3.25 & -0.25 & -0.11 \\ -0.11 & 3.25 & -0.25 \\ -0.25 & -0.11 & 3.25 \end{pmatrix}$ | $\begin{pmatrix} 3.41 & 0.00 & 0.00 \\ 0.00 & 3.08 & -0.08 \\ 0.00 & 0.08 & 3.08 \end{pmatrix}$ | $\begin{pmatrix} -1.93 & 0.08 & -0.29 \\ 0.11 & -1.65 & 0.12 \\ -0.38 & 0.15 & -2.20 \end{pmatrix}$ |
| An. | $\begin{pmatrix} 2.40 & 0.00 & 0.00 \\ 0.00 & 2.32 & 0.11 \\ 0.00 & 0.11 & 2.32 \end{pmatrix}$ | $\begin{pmatrix} 3.81 & -0.34 & -0.09 \\ -0.09 & 3.81 & -0.34 \\ -0.34 & -0.09 & 3.81 \end{pmatrix}$ | $\begin{pmatrix} 3.87 & 0.00 & 0.00 \\ 0.00 & 3.51 & -0.59 \\ 0.00 & 0.59 & 3.51 \end{pmatrix}$ | $\begin{pmatrix} -1.98 & 0.07 & -0.45 \\ 0.11 & -1.65 & -0.06 \\ -0.62 & 0.16 & -2.78 \end{pmatrix}$ |

X is Mg for pyrope, and Ca for grossular and andradite; Y is Al for pyrope and grossular and Fe for andradite. The fractional coordinates of the reported atoms are: $(\frac{1}{8}, 0, \frac{1}{4})$ for X, $(0, 0, 0)$ for Y and $(\frac{3}{8}, 0, \frac{1}{4})$ for Si; the reported tensor refers to the oxygen whose coordinates are given in Table 1.

where $M_\alpha$ is the mass of atom $\alpha$. The $W$ matrix is diagonalized; the square root of its eigenvalues provide the TO vibrational frequencies, whereas its eigenvectors are used to compute the dipole moment variation along the modes [see Eq. (4-7) below] that is proportional to the mode intensity. Eigenvectors are also used for the graphical representation of the atomic motion in the modes (see www.crystal.unito.it/prtfreq/jmol.html). Moreover, once the Hessian matrix $H$ is calculated, frequency shifts due to isotopic substitutions can readily be obtained simply by changing the masses in the above formula. This allows the calculation of the isotopic-shift at no computational cost.

Energy first derivatives of the total energy $V$ with respect to atomic positions, $\upsilon_{\alpha j} = \partial V / \partial u_{\alpha j}$ are calculated analytically for all $u_{\alpha j}$ coordinates ($u_{\alpha j}$ is the displacement coordinate with respect to the equilibrium), whereas second derivatives at $u_{\alpha j} = 0$ are calculated numerically as follows:

$$\left[\frac{\partial \upsilon_{\alpha j}}{\partial u_{\beta i}}\right]_0 \approx \frac{\upsilon_{\alpha j}(0, \cdots, u_{\beta i}, \cdots) - \upsilon_{\alpha j}(0, \cdots, 0, \cdots)}{u_{\beta i}} \qquad (3)$$

The displacements ($u_{\beta i}$) with respect to the equilibrium position adopted in our calculations are 0.001 Å (pyrope and grossular) and 0.003 Å (andradite). Previous studies[4,22] confirmed that frequencies obtained with these two values differ by less than 1 $cm^{-1}$.

### *The Born Charges*

Atomic Born tensors are the key quantity for the calculation of longitudinal optical (LO) modes, IR intensities and the static dielectric tensor. They are defined as follows:

$$Z^*_{\alpha,ij} = \frac{\partial}{\partial u_{\alpha j}}\left(\frac{\partial V}{\partial E_i}\right) \equiv \frac{\partial}{\partial u_{\alpha j}}\mu_i \qquad (4)$$

where $E_i$ is a component of an applied electric field and $\mu_i$ is the $i$-th component of the cell dipole moment.

It is well known[23] that, in crystalline systems, $\vec{\mu}$ is not a bulk property, so that it cannot be determined per unit cell because its value precisely depends on the arbitrary choice of the cell. On the contrary, the dipole moment difference between two geometries of the same system (i.e., the polarization per unit cell) is an observable in periodic systems. Consequently, partial derivatives in eq. (4) are estimated numerically from the polarizations generated by small atomic displacements as in the calculation of the energy second derivatives [see eq. (3)]. Polarization is computed by means of the localized Wannier Functions (WF)[24–27] as the difference between the sum of the reference WF centroids at two geometries: In the present case, the equilibrium geometry and each one of the distorted geometries used in the numerical derivative scheme.

The procedure for the calculation of the polarization derivatives is as follows. The complete localization scheme[24] is performed only once for the central (equilibrium) point, and the centroids of the resulting WFs are computed in the usual way. As concerns the distorted structures, the WFs are obtained by projecting those obtained for the undistorted structure onto the corresponding occupied manifold, then the centroids are calculated. Owing to the small geometry differences between the central and the displaced points in the atomic coordinate space, the projection technique allows us to obtain localized enough WFs suitable for an accurate computation of the polarization.

The $Z^*_\alpha$ atomic Born tensors obtained in this way for the nonequivalent atoms of pyrope, grossular, and andradite are given in Table 2.

### *The IR Intensity and the Dielectric Tensors*

It is convenient to represent the Born charge tensors in the basis of vibrational modes. The eigenvectors matrix $T$ of the mass-weighted Hessian matrix $W$ that transforms the cartesian atomic directions $\mathbf{u}_{\alpha j}$ into the $p$-th normal coordinate direction, $\mathbf{Q}_p$, through a suitable mass-weighting factor:

$$\mathbf{Q}_p = \sum_{\alpha i} (t_{p,\alpha i}/\sqrt{M_\alpha})\mathbf{u}_{\alpha i} \qquad (5)$$

is used to transform the Born charges, too:

$$\bar{Z}_{p,i} = \sum_{\alpha j} t_{p,\alpha j} Z^*_{\alpha,ij}/\sqrt{M_\alpha}. \qquad (6)$$

**Table 3.** Born Charges $\bar{Z}_m$ ($|e|$) in the Normal Mode Basis for the IR Active Modes and Contributions to the Static Dielectric Tensor $\varepsilon^0$ ($k_m = 4\pi/\Omega_0 \times \bar{Z}_m^2/\omega_m^2$) for Pyrope, Grossular, and Andradite.

| Pyrope | | | Grossular | | | Andradite | | |
|---|---|---|---|---|---|---|---|---|
| $\nu$ | $\bar{Z}_m$ | $k_m$ | $\nu$ | $\bar{Z}_m$ | $k_m$ | $\nu$ | $\bar{Z}_m$ | $k_m$ |
| 121.2 | 0.996 | 4.323 | 153.4 | 0.317 | 0.246 | 125.4 | 0.255 | 0.225 |
| 139.8 | −0.091 | 0.027 | 183.7 | −0.567 | 0.551 | 148.5 | 0.294 | 0.213 |
| **189.4** | **−1.067** | **2.030** | 206.9 | 0.332 | 0.149 | 184.0 | −0.625 | 0.628 |
| 215.8 | 0.054 | 0.004 | 242.0 | 0.634 | 0.397 | 206.3 | 0.509 | 0.330 |
| 259.9 | 0.496 | 0.233 | 303.2 | 0.507 | 0.162 | 243.7 | 0.267 | 0.065 |
| **334.3** | **−1.467** | **1.232** | 357.5 | 0.235 | 0.025 | 271.4 | 0.196 | 0.028 |
| 348.6 | −0.171 | 0.015 | **394.6** | **−1.770** | **1.164** | **288.0** | **2.269** | **3.375** |
| **382.9** | **−1.102** | **0.530** | 407.0 | −0.080 | 0.002 | 313.8 | 0.087 | 0.004 |
| 423.1 | 0.669 | 0.160 | 424.2 | −0.173 | 0.010 | 340.2 | −0.744 | 0.260 |
| **459.1** | **2.166** | **1.424** | **441.0** | **−2.609** | **2.025** | **366.2** | **1.711** | **1.186** |
| 483.7 | 0.508 | 0.070 | 480.8 | 0.334 | 0.028 | 433.2 | 0.808 | 0.189 |
| 532.9 | 0.545 | 0.067 | 509.3 | −0.225 | 0.011 | 473.4 | −0.620 | 0.093 |
| 582.9 | −0.673 | 0.085 | 546.4 | −0.503 | 0.049 | 503.0 | −0.871 | 0.163 |
| 674.1 | 0.039 | 0.000 | 625.9 | 0.503 | 0.037 | 588.4 | 0.230 | 0.008 |
| **864.8** | **2.190** | **0.410** | **829.6** | **2.362** | **0.469** | **794.3** | **2.728** | **0.641** |
| **896.0** | **−1.390** | **0.154** | **849.6** | **−1.038** | **0.086** | **813.3** | **−1.626** | **0.217** |
| **969.8** | **1.398** | **0.133** | **901.8** | **1.508** | **0.162** | **869.6** | **1.749** | **0.220** |

Rows corresponding to $\bar{Z}_m$ values larger than one are in bold.

Intensity of the $p$-th IR mode can be written as follows:

$$A_p \propto d_p \left| \frac{\partial \vec{\mu}}{\partial Q_p} \right|^2 \tag{7}$$

being proportional to the square of the modulus of the first derivative of the dipole moment $\vec{\mu}$ with respect to displacement $Q_p$ along the normal mode direction $\vec{Q}_p$ times the $d_p$ degeneracy of the mode. Because of eqs. (4) and (6), it can also be written as:

$$A_p \propto d_p \sum_j \bar{Z}_{p,j}^2; \tag{8}$$

In the present case, the $\bar{Z}_p$ vectors are non-null only for the 17 IR active $F_{1u}$ modes. Three degenerate vectors associated with each mode are polarized along $x$, $y$, and $z$, respectively, so that only one component of each $\bar{Z}_p$ is non-null. These values are given in Table 3.

To calculate the static dielectric constant $\varepsilon^0$, the ionic contribution, obtained from the frequency eigenvalues ($\omega_p$) and the $\bar{Z}_p^*$ vectors, is added to $\varepsilon^\infty$:

$$\varepsilon_{ij}^0 = \varepsilon_{ij}^\infty + \frac{4\pi}{\Omega} d_p \sum_p \frac{\bar{Z}_{p,i}\bar{Z}_{p,j}}{\omega_p^2} \tag{9}$$

where $\Omega$ is the unit cell volume. As only one component of $\bar{Z}_p$ is non-null, the tensor reduces to a constant matrix and Eq. (9) simplifies to:

$$\varepsilon_{ii}^0 = \varepsilon_{ii}^\infty + \frac{4\pi}{\Omega} d_p \sum_p \frac{\bar{Z}_{p,i}^2}{\omega_p^2}. \tag{10}$$

The static dielectric constant is then obtained by adding the 17 $F_{1u}$ contributions only to $\varepsilon^\infty$ (see Table 3). The vibrational contribution to $\varepsilon^0$ is different for the three compounds: about 11 for pyrope, (the mode at 121.2 $cm^{-1}$ provides the largest addendum, followed by modes at 189.0, 334.3, and 459.1 $cm^{-1}$), 7.5 for andradite (with only two important terms, from modes at 441.0 and 394.6 $cm^{-1}$), and only 5.8 for grossular (also in this case only two important contributions, from modes at 288.0 and 366.2 $cm^{-1}$).

The electronic (clamped nuclei) dielectric constant $\varepsilon^\infty$, was evaluated by using a finite field saw-tooth model,[28] which requires the use of supercells large enough to eliminate border effects because of the change of sign of the applied electric field. Calculations for the present compounds were performed with supercells containing 320 atoms. The resulting dielectric constants were found to be stable within 0.001 with respect to larger supercells. The intensity of the applied electric field was 0.001 a.u. ($5.142 \times 10^8$ V/m).

The static and high frequency dielectric constants for the three systems are given in Table 4. Agreement with experiments is in general very satisfactory with an average absolute difference of 6%. In particular, $\varepsilon^\infty$ for the three garnets is underestimated, whereas $\varepsilon^0$ for pyrope and andradite is overestimated.

### *The Nonanalytical Contribution and the LO Modes*

The second term in the rhs of eq. (1) depends on the direction of the momentum $\mathbf{k} \equiv k_m$ exchanged with the radiation field (see ref. 31 sections 5, 10, 34, 35; and ref. 32):

$$W_{\alpha i,\beta j}^{\mathrm{NA}}(\mathbf{k} \to \mathbf{0}) = \frac{4\pi}{\Omega} \frac{\left(\sum_m k_m Z_{\alpha,mi}^*\right)\left(\sum_n k_n Z_{\beta,nj}^*\right)}{\sqrt{M_\alpha M_\beta}\left(\sum_{m,n} k_m \varepsilon_{mn}^\infty k_n\right)}, \tag{11}$$

Equation (1) can be rewritten in the basis of the $\mathbf{Q}_p$ vectors as Eqs. (5) and (6), giving rise to

$$\bar{W}_{pq}(\mathbf{k} \to \mathbf{0}) = \delta_{pq}\omega_p + \frac{4\pi}{\Omega} \frac{\left(\sum_m \bar{Z}_{p,m} k_m\right)\left(\sum_n \bar{Z}_{q,n} k_n\right)}{\sum_{mn} k_m \varepsilon_{mn}^\infty k_n}, \tag{12}$$

where $\omega_p$ is the $p$-th eigenvalue of the analytic DM.

**Table 4.** Calculated and Experimental Static ($\varepsilon^0$) and High Frequency ($\varepsilon^\infty$) Dielectric Constants.

| | $\varepsilon^0$ | | | $\varepsilon^\infty$ | | |
|---|---|---|---|---|---|---|
| System | Calc. | Exp. | Δ% | Calc. | Exp. [b] | Δ% |
| Pyrope | 13.62 | 12.35 | +10 | 2.72 | 3.06 | −11 |
| Grossular | 8.53 | 8.58 | −0.6 | 2.76 | 2.96 | −7 |
| Andradite | 10.85 | 10.53 | +3 | 3.36 | 3.53 | −5 |

[a] Ref. 29.
[b] Ref. 30.

When an irreducible representation (IRREP) of the little symmetry group of the system at the Γ-point[33] ($\bar{G}_\Gamma$) is contained in the coordinate space $R^3$ only once, a set of wave-vectors **k** can be chosen such that the nonanalytic term vanishes except in those cases where $\mathbf{t}_p$, $\mathbf{t}_q$, and **k** belong to the same IRREP row, as it is the case here, where they belong to the three rows of $F_{1u}$.

Accordingly, the last term in the rhs of Eq. (12), in the basis of the IRREPs contained in $R^3$ $\{\gamma_r\}$, is factorized into few nonvanishing matrices, each corresponding to a row of the $\gamma_r$-IRREPs of $\bar{G}_\Gamma$,

$$\bar{W}^{(\gamma_r)}_{p,q}(\mathbf{k}^{(\gamma_r),w} \to \mathbf{0}) = \delta_{pq}\omega^{(\gamma_r)}_p + \frac{4\pi}{\Omega}\frac{\left(\sum_m \bar{Z}^{(\gamma_r,w)}_{p,m} k^{(\gamma_r,w)}_m\right)\left(\sum_n \bar{Z}^{(\gamma_r,w)}_{q,n} k^{(\gamma_r,w)}_n\right)}{\sum_{m,n} k^{(\gamma_r,w)}_m \varepsilon^{\infty}_{mn} k^{(\gamma_r,w)}_n}, \quad (13)$$

where now $p, q$ run over those modes that belong to row $w$ of IRREP $\gamma_r$, and $\mathbf{k}^{(\gamma_r,w)}$ denotes each of the three symmetry adapted basis vectors of the $R^3$ space.

In those cases where the nonanalytic part vanishes, it is said that the wave vector **k** and the polarization $\bar{Z}_{p,m}$ are perpendicular and the resulting modes (eigenvectors of the analytic part) are the so-called Transverse Optical (TO) modes. If this is not the case, the phonon wave vector and the polarization are parallel, leading to a nonanalytic correction to the DM and giving rise to the so-called Longitudinal Optical (LO) modes.

It is worth noticing that matrix elements of $\bar{W}^{(\gamma_r)}_{p,q}(\mathbf{k}^{(\gamma_r,w)} \to \mathbf{0})$ do not actually depend on $w$, the chosen row of the $\gamma_r$-IRREP. Therefore, only one matrix for IRREP needs to be diagonalized to obtain the LO (and TO) frequencies. The set of modes belonging to the other rows can be obtained by using appropriate shift operators of the IRREPs.

A particular case appears when two one–dimensional IRREPs, namely $\gamma_r$ and $\gamma_{r^*}$, are complex conjugate to each other (time reversal real pairing[33]). As vibrational modes are real, both IRREPs must be directly summed into a single two-dimensional representation $\bar{\gamma}_r = \gamma_r \oplus \gamma_{r^*}$, irreducible in real space. In this context, there are strictly no rows and, obviously, no shift operators to exchange them. As a matter of fact, if the basis set used to represent the DM in eq. (13) is real, both conjugate IRREPs show the same real form of the non analytic part.

$$\begin{aligned}
&\bar{W}^{(\gamma_r)}_{p,q}(\mathbf{k}^{(\gamma_r)} \to \mathbf{0}) \\
&= \delta_{pq}\omega^{(\bar{\gamma}_r)}_p + \frac{4\pi}{\Omega}\frac{\left(\sum_m \bar{Z}^{(\gamma_r)}_{p,m} k^{(\gamma_r)}_m\right)\left(\sum_n \bar{Z}^{(\gamma_r)}_{q,n} k^{(\gamma_r)}_n\right)^*}{\sum_{mn} k^{(\gamma_r)}_m \varepsilon^{\infty}_{mn} k^{(\gamma_r)*}_n} \\
&= \delta_{pq}\omega^{(\bar{\gamma}_r)}_p + \frac{4\pi}{\Omega} \\
&\times \frac{\left(\sum_m \bar{Z}^{(\bar{\gamma}_r)}_{p,m} a^{(\bar{\gamma}_r)}_m\right)\left(\sum_n \bar{Z}^{(\bar{\gamma}_r)}_{q,n} a^{(\bar{\gamma}_r)}_n\right) + \left(\sum_m \bar{Z}^{(\bar{\gamma}_r)}_{p,m} b^{(\bar{\gamma}_r)}_m\right)\left(\sum_n \bar{Z}^{(\bar{\gamma}_r)}_{q,n} b^{(\bar{\gamma}_r)}_n\right)}{\sum_{mn}\left(a^{(\bar{\gamma}_r)}_m \varepsilon^{\infty}_{mn} a^{(\bar{\gamma}_r)}_n\right) + \left(b^{(\bar{\gamma}_r)}_m \varepsilon^{\infty}_{mn} b^{(\bar{\gamma}_r)}_n\right)} \\
&= \bar{W}^{(\gamma_{r^*})}_{p,q}(\mathbf{k}^{(\gamma_{r^*})} \to \mathbf{0}) = W^{(\bar{\gamma}_r)}_{p,q}(\mathbf{a}^{(\bar{\gamma}_r)} + i\mathbf{b}^{(\bar{\gamma}_r)} \to \mathbf{0}) \quad (14)
\end{aligned}$$

where $k^{(\gamma_r)}_m = k^{(\gamma_{r^*})^*}_m = a^{(\bar{\gamma}_r)}_m + ib^{(\bar{\gamma}_r)}_m$, $m = 1, 2, 3$. Equation (14) provides the expression of the DM for the real paired $\bar{\gamma}_r$-IRREP.

The square roots of the eigenvalues of the $W + W^{NA}$ matrix are the LO frequencies. The eigenvectors can be used for obtaining relative intensities [see Eqs. (4–7)] and mode animations.

In those cases where the non-analytic part $W^{NA}$ is small compared to the analytic part, it is generally easy to find a one-to-one correspondence between TO and LO modes (obviously, this is also the case of one mode per IRREP or per row of IRREP), and the so called TO–LO splitting is determined by ordering the two sets on increasing wavenumbers.

However, when the nonanalytic part is large and alters the DM significantly, the one-to-one correspondence is lost. In those cases, an alternative strategy can be used based on the maximum overlap between the LO and TO modes. It must be, however, taken into account that the TO–LO overlap matrix is not symmetric as TO and LO vectors do not belong to the same orthonormal set because they are originated from independent diagonalizations. Therefore, it can happen that one TO mode may overlap to a LO mode maximally, but not vice versa, preventing from establishing a one-to-one correspondence. Two other criteria, based on the similarity of the isotopic shift among LO and TO modes or on the direct inspection of the modes through animation, can also be used to establish the LO–TO connection.

Because Table 4 shows that there is a difference of 5-10% between calculated and experimental $\varepsilon^{\infty}$, it is important to check how far this may affect calculated LO frequencies. Table 5 reports the LO pyrope wavenumbers for three different $\varepsilon^{\infty}$ values, one close to the experimental determination (3.0), one at the calculated value

**Table 5.** Dependence of the Pyrope Longitudinal Optical (LO) Frequencies on the Value of the High Frequency Dielectric Constant ($\varepsilon^{\infty}$).

| $\varepsilon^{\infty} = 2.50$ | | $\varepsilon^{\infty} = 3.00$ | | $\varepsilon^{\infty}_{calc} = 2.72$ |
|---|---|---|---|---|
| $\nu$ | $\Delta\nu$ | $\nu$ | $\Delta\nu$ | $\nu$ |
| 138.8 | 0.1 | 138.6 | −0.1 | 138.7 |
| 142.1 | 0.2 | 141.7 | −0.2 | 141.9 |
| 214.0 | 0.4 | 213.0 | −0.6 | 213.6 |
| 216.5 | 0.1 | 216.3 | −0.1 | 216.4 |
| 264.2 | 0.1 | 264.0 | −0.1 | 264.1 |
| 348.2 | 0.0 | 348.1 | −0.1 | 348.2 |
| 355.2 | 0.3 | 354.5 | −0.4 | 354.9 |
| 397.7 | 0.3 | 397.0 | −0.4 | 397.4 |
| 426.7 | 0.1 | 426.5 | −0.1 | 426.6 |
| 482.3 | 0.0 | 482.3 | 0.0 | 482.3 |
| 527.2 | 0.4 | 526.3 | −0.5 | 526.8 |
| 566.9 | 1.5 | 563.3 | −2.1 | 565.4 |
| 625.3 | 5.2 | 614.3 | −5.8 | 620.1 |
| 674.2 | 0.0 | 674.2 | 0.0 | 674.2 |
| 885.3 | 0.2 | 884.8 | −0.3 | 885.1 |
| 941.1 | 1.5 | 937.6 | −2.0 | 939.6 |
| 1071.6 | 14.0 | 1043.5 | −14.1 | 1057.6 |
| $\lvert\bar{\Delta}\rvert$ | 1.4 | | 1.6 | |
| $\bar{\Delta}$ | 1.4 | | −1.6 | |
| $\Delta_{\min}$ | 0.0 | | −14.1 | |
| $\Delta_{\max}$ | 14.0 | | 0.0 | |

$\Delta\nu$ values are calculated with respect to the (LO) frequencies obtained using the computed $\varepsilon^{\infty}$ (see Table 4).

(2.72) and the third about 10% lower than the latter. It turns out that only two frequencies of the set are affected by more than 2 $cm^{-1}$ (5.8 and 14.1 $cm^{-1}$), confirming that the amount of LO shift is not dramatically dependent on $\varepsilon^{\infty}$.

### *Statistics and Animation*

Calculated TO and LO frequencies $\nu_v$ have been compared to experimental sets of $M$ frequencies $\nu_v^{ref}$ through four global indices defined as follows:

$$\overline{|\Delta|} = M^{-1} \sum_{v=1}^{M} \left| \nu_v - \nu_v^{ref} \right|$$

$$\bar{\Delta} = M^{-1} \sum_{v=1}^{M} \nu_v - \nu_v^{ref} \qquad (15)$$

$$\begin{aligned} \Delta_{\max} &= \max\left(\nu_v - \nu_v^{ref}\right) \\ \Delta_{\min} &= \min\left(\nu_v - \nu_v^{ref}\right) \end{aligned} \qquad v = 1, 2, \ldots M$$

where, $\overline{\Delta}$, $\overline{|\Delta|}$, $\Delta_{\max}$, and $\Delta_{min}$ (all in $cm^{-1}$) are the average of the difference, the average of the absolute difference, and the maximum and minimum difference.

Visualization of structures has been dealt with the MOLDRAW program[34] and animations of the modes have been obtained by using the molecular viewer JMOL[35] from input files prepared by MOLDRAW. This would help to highlight the differences between the present simulated modes and the ones obtained simply from symmetry analysis.

## The IR Spectrum to and LO Vibrational Results

The decomposition of the reducible representation built on the basis of the cartesian coordinates of the atoms in the unit cell leads to the following symmetry assignment of the 240 normal modes (this analysis is performed automatically by the CRYSTAL06 code): $\Gamma_{\text{total}} = 3A_{1g} + 5A_{2g} + 8E_g + 14F_{1g} + 14F_{2g} + 5A_{1u} + 5A_{2u} + 10E_u + 18F_{1u} + 16F_{2u}$. 55 modes are inactive, 25 are Raman active ($3A_{1g} + 8E_g + 14F_{2g}$ symmetries) and 17 are IR active ($F_{1u}$ symmetry; one additional $F_{1u}$ mode corresponds to translations). Because a thorough analysis of the whole vibrational spectrum of garnets as well as a rigorous assignment of normal modes were carried out in our previous works,[4,5] only a general description of the calculated 17 infrared active modes of each system is performed in the present paper together with the comparison of both the TO and the LO calculated modes with experiment.

### *General Features of the Calculated Spectrum*

Tables 6, 7, and 8 report the calculated TO and LO modes of pyrope, grossular and andradite, as well as their corresponding intensities. These data are also represented graphically in Figures 1, 2, and 3 to achieve an overall appreciation of similarities and differences of the three spectra. Note that the present graphical representations of the calculated modes cannot be directly compared with the experimental spectra. Their aim is simply to highlight the relative position of the TO and LO peaks. As regards the TO data, the three systems present similar features: peaks appear in two regions separated by a large gap of about 200 $cm^{-1}$. The low frequency part of the spectrum is characterized by two very intense peaks, one in between 300 and 400 $cm^{-1}$, the second at about 450 $cm^{-1}$ (pyrope and grossular) or 350 $cm^{-1}$ (andradite). Intensities of these peaks are about the same for the first two systems, whereas for andradite, relative intensities are reversed. Inspection of the normal mode animations[37] show that the most intense peak (459, 441, and 288 $cm^{-1}$ for pyrope, grossular and andradite, respectively) corresponds to a translation of the octahedrally coordinated central cation (i.e., Al for pyrope and grossular and Fe for andradite) in the three cases. Because Fe is heavier than Al, the vibrational frequency is downshifted by more than 150 $cm^{-1}$. The second most intense peak (334.3, 394.6, and 366.2 $cm^{-1}$ for pyrope, grossular, and andradite, respectively) corresponds to a bending of the octahedron, which implies also a "translation" of the tetrahedra connected to it and is compensated by an opposite translation of the $Mg^{2+}$ and $Ca^{2+}$ cations. The aforementioned cases are good examples of the difficulties in describing garnet spectra due to the mixing between the modes as already discussed in our previous papers on garnets,[4,5] where it was shown that the problem of a rigorous normal mode assignment in these materials cannot be overcome just by considering symmetry analysis, and additional tools (e.g., animations of the normal modes) must be employed in order to obtain a proper description.

The higher frequency part of the spectrum is characterized by three intense bands. The first two are well separated in pyrope, whereas in grossular and andradite they overlap to a certain amount. These three peaks correspond to the antisymmetric stretchings of the $SiO_4$ units. Their absolute position is the highest for pyrope (865–970 $cm^{-1}$ interval), the most compact member of the set (see the lattice parameters and the Si–O bonds in table 1). The band is downshifted by about 30 $cm^{-1}$ for grossular (830–902 $cm^{-1}$) and by 30 more wavenumbers in andradite (794–870 $cm^{-1}$).

The LO part of the spectrum of the three compounds also present similar features and split into two zones, each one showing two intense peaks. For the analysis of the normal modes associated with the LO peaks, we refer to animations in our website.[37]

The apparently different structure of LO and TO parts of the spectra in the plots seem to contradict the similarity observed in the tabulated data. However, it must be remarked that it is the relative intensities rather than the wavenumbers to produce a different appearance of the LO and TO modes.

### *Comparing TO and LO Wavenumbers with Experiment*

Several infrared experimental studies have been reported for garnets. In most of them, incomplete sets (less than 17 modes) have been reported, suggesting that some of the modes are characterized by low intensity.

The paper by Hofmeister et al.[3] is an exception as they provide complete IR sets for pyrope, grossular and andradite obtained from infrared reflectance spectra collected at zero pressure and room temperature in samples with end-member composition. The authors, however, emphasize that the 17 expected bands were

**Table 6.** Calculated and Experimental IR–TO and LO Modes ($F_{1u}$ Symmetry) of Pyrope $Mg_3Al_2Si_3O_{12}$ and Their Calculated Intensity.

| IR-TO modes | | | | IR-LO modes | | | | LO-TO | |
|---|---|---|---|---|---|---|---|---|---|
| $\nu_{cal.}$ | I | $\nu^a_{exp.}$ | $\Delta\nu$ | $\nu_{cal.}$ | I | $\nu^a_{exp.}$ | $\Delta\nu$ | $\delta\nu$ | S |
| 121.2 | 2904 | – (134) | – (−12.8) | 141.9 | 85 | 152 (152) | −10.1 (−10.1) | 20.7 | 73 |
| **139.8** | **24** | **140 (134)** | **−0.2 (5.8)** | **138.7** | **38** | **– (152)** | **– (−13.3)** | **−1.1** | 79 |
| 189.4 | 3330 | 200 (195) | −10.6 (−5.6) | 213.6 | 302 | – (218) | – (−4.4) | 24.2 | 83 |
| 215.8 | 8 | 238 (221) | −22.2 (−5.2) | 216.4 | 80 | 218 (223) | – 1.6 (−6.6) | 0.6 | 91 |
| 259.9 | 720 | 260 (259) | −0.1 (0.9) | 264.1 | 98 | 263 (263) | 1.1 (1.1) | 4.2 | 97 |
| 334.3 | 6296 | 339 (336) | −4.7 (−1.7) | 354.9 | 326 | 353 (357) | 1.9 (−2.1) | 20.6 | 81 |
| **348.6** | **85** | **365 (336)** | **−16.4 (12.6)** | **348.2** | **19** | **– (357)** | **– (−8.8)** | **−0.4** | 95 |
| 382.9 | 3552 | 385 (383) | −2.1 (−0.1) | 397.4 | 391 | 400 (399) | −2.6 (−1.6) | 14.5 | 84 |
| 423.1 | 1309 | 423 (422) | 0.1 (1.1) | 426.6 | 93 | 422 (423) | 4.6 (3.6) | 3.5 | 93 |
| 459.1 | 13721 | 458 (455) | 1.1 (4.1) | 526.8 | 603 | 528 (529) | −1.2 (−2.2) | 67.7 | 35 |
| **483.7** | **753** | **478 (478)** | **5.7 (5.7)** | **482.3** | **32** | **474 (475)** | **8.3 (7.3)** | **−1.4** | 97 |
| 532.9 | 869 | 536 (535) | −3.1 (−2.1) | 565.4 | 2691 | 556 (557) | 9.4 (8.4) | 32.5 | 91 |
| 582.9 | 1326 | 583 (581) | −0.1 (1.9) | 620.1 | 9535 | 618 (620) | 2.1 (0.1) | 37.2 | 75 |
| 674.1 | 4 | 664 (∼650) | 10.1 (24.1) | 674.2 | 14 | 667 (–) | 7.2 (–) | 0.1 | 100 |
| 864.8 | 14028 | 878 (871) | −13.2 (−6.2) | 939.6 | 4506 | 940 (941) | −0.4 (−1.4) | 74.8 | 47 |
| **896.0** | **5648** | **906 (902)** | **−10.0 (−6.0)** | **885.1** | **583** | **889 (890)** | **−3.9 (−4.9)** | **−10.9** | 75 |
| 969.8 | 5712 | 976 (972) | −6.2 (−2.2) | 1057.6 | 40961 | 1063 (1060) | −5.4 (−2.4) | 87.8 | 69 |
| $\|\Delta\|$ | | 6.6 (5.8) | | | | 4.3 (4.9) | | | |
| $\bar{\Delta}$ | | −4.5 (−0.8) | | | | 0.7 (−2.3) | | | |
| $\Delta_{min}$ | | −22.2 (−12.8) | | | | −10.1 (−13.3) | | | |
| $\Delta_{max}$ | | 10.1 (24.1) | | | | 9.4 (8.4) | | | |

The calculated high frequency dielectric constant reported in Table 4 has been used. $\Delta\nu$ is the difference between the calculated and the experimental data. $\delta\nu$ is the calculated LO–TO splitting. $S$ is the absolute value of the overlap between the TO and LO eigenvectors multiplied by $10^2$. Frequencies and differences in $cm^{-1}$ and intensities in km/mol.
[a]Ref. 3. In parenthesis data from ref. 10.

directly observed only for pyrope, whereas for grossular and andradite only 14 and 16 bands, respectively, could be identified clearly. The sets of the latter garnets were therefore completed to 17 by applying different experimental techniques in order to reveal the missing peaks.

In spite of the completeness of these experimental sets, it has not always been possible to establish a one-to-one correspondence between simulated and measured wavenumbers. Among the pyrope TO modes, for example, a peak is observed at 279 $cm^{-1}$ with no theoretical counterpart. Thus, this experimental peak seems to have been added to complete the set on the basis of indirect observations, rather than strong experimental evidence.

Similar considerations apply to the three pyrope LO experimental peaks at 240, 280, and 370 $cm^{-1}$ not appearing in the simulated spectrum. Vice versa, the calculated peaks at 139.7, 213.6, and 348.2 $cm^{-1}$ are not observed in the experiment. For grossular, only one TO and one LO anomalous cases are observed ($TO^{exp}$: 245, $TO^{calc}$: 407.0; $LO^{exp}$: 249 and $LO^{calc}$: 407.9, values in $cm^{-1}$). For andradite, a single discrepancy is noticed in the set ($LO^{exp}$: 332, $LO^{calc}$: 271.5, values in $cm^{-1}$). These qualitative, rather than quantitative discrepancies, seem then to be due to difficulties encountered on the experimental side to fill the expected list of 17 peaks. As a matter of fact, the experimental determination can be affected by many problems, including low intensity, overtones and background effects, whereas all calculated peaks are characterized by about the same accuracy, irrespective of their position in the spectrum and of their intensity, so that it is not expected that one individual peak is affected by larger errors.

The comparison between experimental and calculated TO and LO modes (see Tables 6, 7 and 8) after the exclusion of the peaks just mentioned, deserves few comments:

- The agreement between calculation and experiment for the six sets (TO and LO sets for each of the three systems; overall, more than 100 data) is excellent: the mean absolute errors ($|\bar{\Delta}|$) are 6.6, 5.8, and 6.9 $cm^{-1}$ (TO sets) and 4.3, 3.8, and 6.1 $cm^{-1}$ (LO). The difference exceeds 20 $cm^{-1}$ only in two cases, and it is larger than 15 $cm^{-1}$ only in four cases.
- Cases exhibiting the largest difference between calculation and experiment generally correspond to low intensity modes. Consider, for instance, the four pyrope TO modes (in $cm^{-1}$) with the lowest computed intensities I (in km/mol): 674.1 (I = 4), 215.8 (I = 8) 139.8 (I = 24), and 348.6 (I = 85). Of these, the one computed at 215.8 $cm^{-1}$ shows the largest difference among theory and experiment (−22.2 $cm^{-1}$). Similarly, the peak computed at 348.6 $cm^{-1}$ differs from the experimental datum by −16.4 $cm^{-1}$, which is the second largest discrepancy, and that at 674.1 $cm^{-1}$ shows a difference of 10.1 (fifth largest difference). This agreement is, however, not confirmed in a more recent experimental set[10](values in parenthesis of Table 6), where it is claimed that only a weak band at about 650 $cm^{-1}$ was detected in that zone, giving a difference of 24.1 $cm^{-1}$ with the calculated TO frequency.

**Table 7.** Same as Table 6 for Grossular $Ca_3Al_2Si_3O_{12}$.

| IR-TO modes | | | | IR-LO modes | | | | LO-TO | |
|---|---|---|---|---|---|---|---|---|---|
| $\nu_{cal.}$ | Intensity | $\nu^{a}_{exp.}$ | $\Delta\nu$ | $\nu_{cal.}$ | Intensity | $\nu^{a}_{exp.}$ | $\Delta\nu$ | $\delta\nu$ | S |
| 153.4 | 293 | 159 (156) | −5.6 (−2.6) | 155.2 | 20 | 159 (158) | −3.8 (−2.8) | 1.8 | 99 |
| 183.7 | 940 | 186 (184) | −2.3 (−0.3) | 189.0 | 77 | 189 (189) | 0.0 (0.0) | 5.3 | 98 |
| 206.9 | 323 | 205 (205) | 1.9 (1.9) | 208.9 | 41 | 207 (207) | 1.9 (1.9) | 2.0 | 98 |
| 242.0 | 1176 | 245 (241) | −3.0 (1.0) | 248.0 | 135 | 249 (249) | −1.0 (−1.0) | 6.0 | 98 |
| 303.2 | 751 | 302 (301) | 1.2 (2.2) | 305.8 | 62 | 303 (303) | 2.8 (2.8) | 2.6 | 99 |
| 357.5 | 162 | 356 (355) | 1.5 (2.5) | 357.8 | 5 | 357 (356) | 0.8 (1.8) | 0.3 | 100 |
| 394.6 | 9164 | 399 (390) | −4.4 (4.6) | 407.9 | 142 | − (−) | − (−) | 13.3 | 76 |
| **407.0** | **19** | **− (−)** | **− (−)** | **406.7** | **36** | **406 (405)** | **0.7 (1.7)** | **−0.3** | 88 |
| 424.2 | 88 | ∼430 (∼425) | −5.8 (−0.8) | 424.2 | 1 | ∼425 (−) | −0.8 (−) | 0.0 | 100 |
| 441.0 | 19910 | 449 (435) | −8.0 (6.0) | 539.2 | 1288 | 530 (529) | 9.2 (10.2) | 98.2 | 38 |
| **480.8** | **326** | **474 (471)** | **6.8 (9.8)** | **480.1** | **26** | **468 (470)** | **12.1 (10.1)** | **−0.7** | 99 |
| **509.3** | **149** | **505 (506)** | **4.3 (3.3)** | **508.6** | **64** | **503 (506)** | **5.6 (2.6)** | **−0.7** | 99 |
| 546.4 | 741 | 542 (540) | 4.4 (6.4) | 583.1 | 8820 | 579 (576) | 4.1 (7.1) | 36.7 | 44 |
| 625.9 | 739 | 618 (618) | 7.9 (7.9) | 634.4 | 2641 | 631 (624) | 3.4 (10.4) | 8.5 | 93 |
| 829.6 | 16321 | 843 (838) | −13.4 (−8.4) | 879.8 | 2497 | 883 (885) | −3.2 (−5.2) | 50.2 | 53 |
| **849.6** | **3149** | **860 (856)** | **−10.4 (−6.4)** | **845.6** | **210** | **850 (851)** | **−4.4 (−5.4)** | **−4.0** | 86 |
| 901.8 | 6653 | 914 (908) | −12.2 (−6.2) | 1002.5 | 44838 | 1010 (1007) | −7.5 (−4.5) | 100.7 | 65 |
| $\lvert\Delta\rvert$ | | 5.8 (4.4) | | | | 3.8 (4.5) | | | |
| $\bar{\Delta}$ | | −2.3 (1.3) | | | | 1.2 (2.0) | | | |
| $\Delta_{min}$ | | −13.4 (−8.4) | | | | −7.5 (−5.4) | | | |
| $\Delta_{max}$ | | 7.9 (9.8) | | | | 12.1 (10.4) | | | |

[a]Ref. 3. In parenthesis ref. 8 Additional experimental sets of 16 TO frequencies[9] and 16 LO-TO pairs,[36] obtained by means of powder infrared spectroscopy, are not reported here as they essentially coincide with the set by McAloon and Hofmeister.[8]

**Table 8.** Same as Table 6 for Andradite $Ca_3Fe_2Si_3O_{12}$.

| IR-TO modes | | | | IR-LO modes | | | | LO-TO | |
|---|---|---|---|---|---|---|---|---|---|
| $\nu_{cal.}$ | Intensity | $\nu^{a}_{exp.}$ | $\Delta\nu$ | $\nu_{cal.}$ | Intensity | $\nu^{a}_{exp.}$ | $\Delta\nu$ | $\delta\nu$ | S |
| 125.4 | 190 | 133 (131) | −7.6 (−5.6) | 126.5 | 12 | 134 (132) | −7.5 (−5.5) | 1.1 | 100 |
| 148.5 | 253 | 152 (151) | −3.5 (−2.5) | 149.7 | 16 | 154 (152) | −4.3 (−2.3) | 1.2 | 100 |
| 184.0 | 1142 | 188 (187) | −4.0 (−3.0) | 187.9 | 58 | 192 (191) | −4.1 (−3.1) | 3.9 | 98 |
| 206.3 | 757 | 213 (213) | −6.7 (−6.7) | 209.1 | 55 | 215 (215) | −5.9 (−5.9) | 2.8 | 98 |
| 243.7 | 209 | 247 (245) | −3.3 (−1.3) | 244.2 | 7 | 246 (245) | −1.8 (−0.8) | 0.5 | 100 |
| 271.4 | 112 | ∼295 (280) | −23.6 (−8.6) | 271.5 | 1 | − (279) | −(−7.5) | 0.1 | 100 |
| 288.0 | 15061 | ∼305 (298) | −17.0 (−10.0) | 323.6 | 576 | 322 (329) | 1.6 (−5.4) | 35.6 | 75 |
| **313.8** | **22** | **324 (322)** | **−10.2 (−8.2)** | **313.7** | **5** | **∼300 (322)** | **13.7 (−8.3)** | **−0.1** | 99 |
| 340.2 | 1620 | 350 (348) | −9.8 (−7.8) | 345.6 | 188 | 359 (355) | −13.4 (−9.4) | 5.4 | 84 |
| 366.2 | 8559 | 374 (374) | −7.8 (−7.8) | 415.6 | 1840 | 418 (416) | −2.4 (−0.4) | 49.4 | 57 |
| 433.2 | 1910 | 433 (432) | 0.2 (1.2) | 454.2 | 2479 | 460 (456) | −5.8 (−1.8) | 21.0 | 65 |
| 473.4 | 1125 | 479 (477) | −5.6 (−3.6) | 482.7 | 1448 | 487 (484) | −4.3 (−1.3) | 9.3 | 79 |
| 503.0 | 2217 | 505 (506) | −2.0 (−3.0) | 528.1 | 6403 | 532 (532) | −3.9 (−3.9) | 25.1 | 80 |
| 588.4 | 154 | 588 (590) | 0.4 (−1.6) | 589.3 | 233 | 592 (591) | −2.7 (−1.7) | 0.9 | 100 |
| 794.3 | 21760 | 795 (807) | −0.7 (−12.7) | 975.2 | 55495 | 970 (982) | 5.2 (−6.8) | 180.9 | 60 |
| **813.3** | **7736** | **822 (825)** | **−8.7 (−11.7)** | **807.5** | **239** | **819 (820)** | **−11.5 (−12.5)** | **−5.8** | 80 |
| **869.6** | **8952** | **876 (880)** | **−6.4 (−10.4)** | **848.7** | **2725** | **858 (858)** | **−9.3 (−9.3)** | **−20.9** | 76 |
| $\lvert\Delta\rvert$ | | 6.9 (6.2) | | | | 6.1 (5.1) | | | |
| $\bar{\Delta}$ | | −6.8 (−6.1) | | | | −3.5 (−5.1) | | | |
| $\Delta_{min}$ | | −23.6 (−12.7) | | | | −13.4 (−12.5) | | | |
| $\Delta_{max}$ | | 0.4 (1.2) | | | | 13.7 (−0.4) | | | |

[a]Ref. 3. In parenthesis ref. 8.

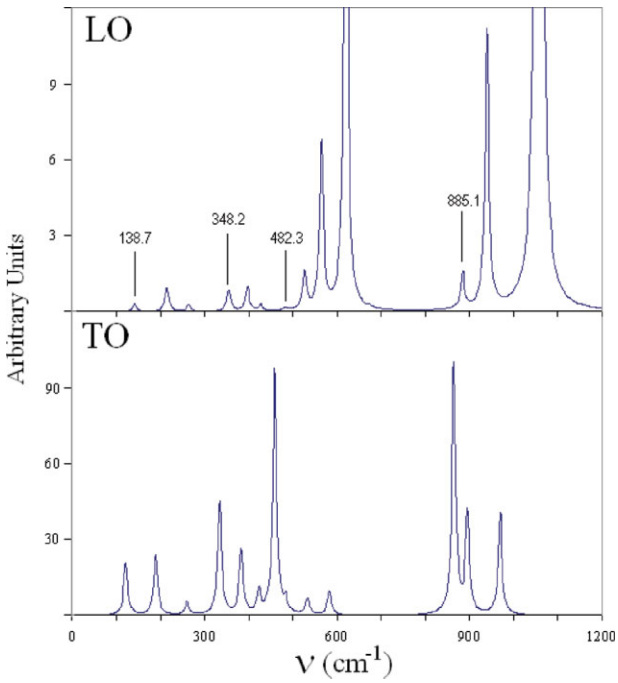


**Figure 1.** LO and TO parts of the calculated infrared spectra of pyrope. A Lorentzian shape (FWHM of 10 $cm^{-1}$) was attributed to each calculated peak. The calculated intensities (in arbitrary units) have been used. The LO intensity scale is one tenth of the TO one. Thus, some of the peaks have been truncated. The LO modes involved in TO-LO "inversions" are indicated. Note that the present graphical representations of the calculated modes cannot be directly compared with the experimental spectra. Their aim is simply to highlight the relative position of the TO and LO peaks, in particular for the discussion of the "inversions" mentioned by Hofmeister.[3]

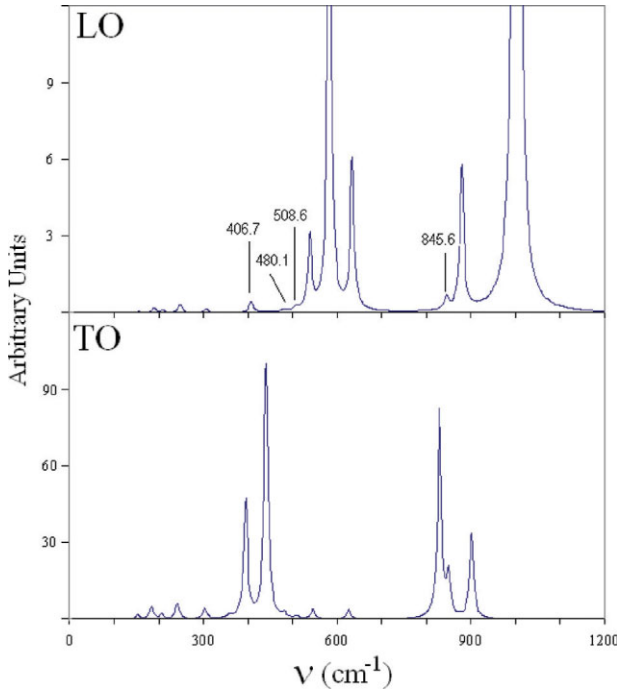


**Figure 2.** LO and TO parts of the calculated infrared spectra of grossular. See Figure 1 for details.

No LO mode corresponding to this low intensity TO peak was detected. This second set of experimental data for pyrope slightly improves the agreement with the present simulation, and differs from the first[3] mainly for the low intensity peaks, as expected.

For grossular and andradite, the situation is similar to the one described for pyrope. For example, in the case of andradite, the largest ($-23.6$ $cm^{-1}$) and third largest ($-10.2$ $cm^{-1}$) differences with the present calculated data are observed for the two peaks with the lowest intensity (see Table 8). More recent experimental data (reflectance spectra collected at room temperature[8]) for grossular and andradite are reported in parentheses in Tables 7 and 8, respectively. They are very similar to the oldest data,[3] the exception being the low intensity peaks now in better agreement with theory (the largest calculated-experimental difference for andradite drops from $-23.6$ to $-11.7$). Overall, the mean absolute difference ($|\bar{\Delta}|$) improves slightly.

- Almost all cases for which no corresponding peaks in the experimental spectra are observed can be explained on the basis of the low calculated intensity: this is the case of the pyrope LO modes at 138.7 (I = 38), 348.2 (I = 19) and 674.2 (I = 14), the latter being present in the oldest set,[3] but not in the most recent one.[10]

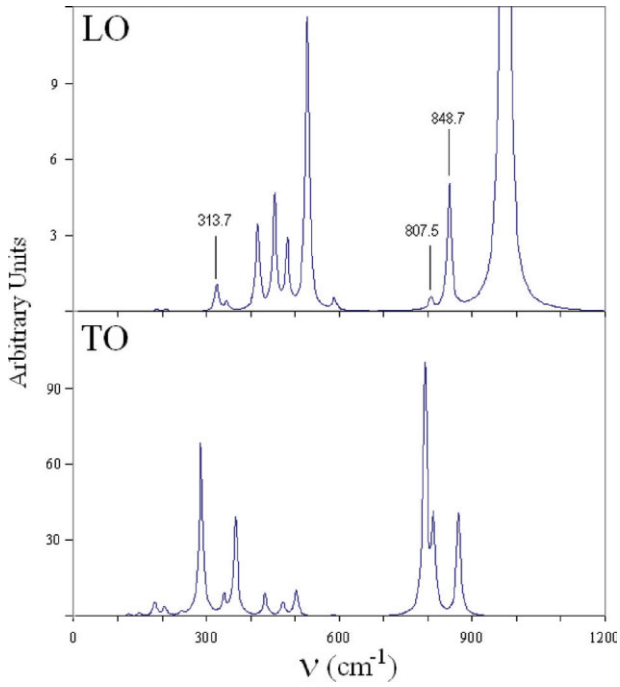


**Figure 3.** LO and TO parts of the calculated infrared spectra of andradite. See Figure 1 for details.

**Table 9.** Effect of the $^{26}$Mg, $^{29}$Al, $^{30}$Si, and $^{18}$O Isotopic Substitution on TO and LO Vibrational Frequencies of Pyrope.

| IR-TO modes | | | | | IR-LO modes | | | | |
|---|---|---|---|---|---|---|---|---|---|
| | $\Delta\nu$ | | | | | $\Delta\nu$ | | | |
| $\nu$ | $^{26}$Mg | $^{29}$Al | $^{30}$Si | $^{18}$O | $\nu$ | $^{26}$Mg | $^{29}$Al | $^{30}$Si | $^{18}$O |
| 121.2 | −3.7 | −0.4 | −0.1 | −0.9 | 141.9 | −7.2 | −0.8 | −0.7 | −2.3 |
| 139.8 | −0.8 | −0.5 | −0.9 | −4.8 | 138.7 | 2.4 | −0.4 | −0.4 | −3.7 |
| 189.4 | −5.8 | −0.1 | −0.5 | −1.5 | 213.6 | −7.2 | −0.2 | −0.6 | −0.2 |
| 215.8 | −2.0 | −0.9 | −0.3 | −7.9 | 216.4 | −1.8 | −1.0 | −0.5 | −8.5 |
| 259.9 | −3.4 | −0.4 | −1.7 | −6.9 | 264.1 | −2.2 | −0.5 | −2.2 | −7.9 |
| 334.3 | −5.4 | −0.8 | −1.4 | −8.4 | 354.9 | −9.1 | −1.9 | −1.1 | −7.3 |
| 348.6 | −0.1 | −1.6 | −1.6 | −14.1 | 348.2 | 3.1 | −2.5 | −1.6 | −14.2 |
| 382.9 | −0.1 | −4.3 | −1.0 | −13.7 | 397.4 | −0.4 | −4.4 | −0.9 | −14.5 |
| 423.1 | −0.2 | −6.9 | −2.5 | −9.2 | 426.6 | −0.4 | −7.4 | −2.4 | −8.2 |
| 459.1 | −0.3 | −10.0 | −0.4 | −11.1 | 526.8 | −0.3 | −2.7 | −3.7 | −19.8 |
| 483.7 | −0.6 | −1.3 | −1.1 | −22.0 | 482.3 | −0.7 | −2.7 | −1.1 | −20.6 |
| 532.9 | −0.1 | −5.9 | −3.8 | −13.2 | 565.4 | −1.7 | −9.4 | −2.5 | −10.3 |
| 582.9 | −0.5 | −7.4 | −2.7 | −15.5 | 620.1 | −0.9 | −7.9 | −1.2 | −18.4 |
| 674.1 | −1.0 | −3.4 | −4.4 | −24.3 | 674.2 | −1.0 | −3.4 | −4.3 | −23.9 |
| 864.8 | 0.0 | 0.0 | −11.6 | −28.9 | 939.6 | −0.5 | −0.2 | −9.7 | −35.5 |
| 896.0 | −0.1 | −0.1 | −11.4 | −31.0 | 885.1 | −0.1 | −0.1 | −12.6 | −28.0 |
| 969.8 | −0.3 | 0.0 | −12.6 | −32.0 | 1057.6 | −0.5 | −1.0 | −14.4 | −32.7 |

### *TO–LO Shifts and Inversions*

In the experimental papers by Hofmeister and collaborators, the problem of the one-to-one correspondence between TO and LO modes (LO-TO splitting or shift) is discussed at length. A pairing scheme with four LO–TO inversions (LO frequency lower than TO) for pyrope, grossular, and andradite was proposed at first.[3] The authors argue that these inversions are observed when a low intensity peak occurs just above a high intensity peak. In more recent experimental studies,[8,10] six out of twelve LO–TO inversions for the three garnets were confirmed. In the only previous theoretical work[38] tackling this point, reversals were excluded on the basis of results produced by using a model potential.

As anticipated in the previous section, the one-to-one correspondence among TO and LO modes is possible without ambiguity only in the cases where a single mode exists for each IRREP of the group at the Γ point; in all other cases LO and TO sets are independent, as resulting from independent diagonalizations of the $W$ and $W + W^{NA}$ matrices [Eqs. (1) and (11)]. In the limit of low polarization, one can however try to establish some correspondence between LO and TO modes, under the hypothesis that $W^{NA}$ modifies only (or mainly) diagonal terms of $W$. To establish such a one-to-one correspondence, despite of arbitrariness, we based our discussion on: (a) overlap criterium, (b) isotopic shift similarity, and (c) inspection of the modes by graphical tools.

TO modes reported in Tables 6, 7, and 8 are ordered by increasing frequency. The LO mode in a given line is the one with the maximum overlap with the TO mode in the same line. The overlap $S$ is given in percent in the last column of the tables. LO frequencies in bold character denotes inversion in the increasing frequency sequence. The $\delta\nu$ column gives the LO–TO splitting evaluated on the basis of the overlap correspondence. It turns out that:

- "Splitting" is never larger than 100 cm$^{-1}$, exceeding 40 cm$^{-1}$ only in 4 out of 17 cases (pyrope).
- Four frequency inversions are observed (bold figures), corresponding to negative "splitting" in all cases (in three cases out of four the negative shift is however smaller than 2 cm$^{-1}$).
- In most cases, the TO–LO overlap is larger than 70%, and the TO–LO correspondence is clearly defined, whereas in two cases pyrope and grossular show overlaps below 50%, which indicates that a large mixing takes place. As expected, these four cases are characterized by large LO-TO shifts, which means that the large $W^{NA}$ diagonal contribution brings about a large mixing with other modes.
- The present data support the observation[3] that the calculated LO–TO inversions occur when a low intensity LO mode is situated just above and very close to a TO mode having high intensity. A representative example is the weak pyrope LO frequency computed at 482.3 cm$^{-1}$ that occurs just above the very strong TO frequency computed at 459.1 cm$^{-1}$. The TO mode corresponding to the LO frequency at 482.3 cm$^{-1}$ (on the basis of the largest overlap) is at 483.7 cm$^{-1}$ with a LO-TO splitting of −1.4 cm$^{-1}$, as reported in Table 6. In Figure 1, this mode and other low intensity LO components of the pairs involved in the inversions are indicated.

The explanation of this behavior is very simple: the TO mode at 483.7 cm$^{-1}$ remains essentially unaltered after the $W^{NA}$ correction. The TO mode at 459.1 cm$^{-1}$ on the other hand shifts by about 67 cm$^{-1}$, so altering the sequence.

The scalar product between pyrope eigenvectors belonging to the TO–LO pair at 482.6–482.3 $cm^{-1}$ is 97% showing that they are very similar. This is confirmed by the frequency shifts due to isotopic substitution reported in Table 9. Essentially the same values ($\sim -0.5$, $\sim -1.0$, and $\sim -20.0$ $cm^{-1}$) are obtained for the LO and TO shifts due to the $^{26}Mg$, $^{30}Si$, and $^{18}O$ isotopes, whereas for $^{29}Al$ shifts are $-1.3$ $cm^{-1}$ for the TO mode and $-2.7$ $cm^{-1}$ for the LO component of the vibration. LO and TO animations[34] provide additional information on the modes, and permit one to justify the observed discrepancy in the $^{29}Al$ isotopic shifts. They show that both components (TO and LO) correspond mainly to distortions of the $SiO_4$ tetrahedra accompanied by aluminum translations inside the octahedron, that are however larger for the LO component with a consequent larger $^{29}Al$ shift. The other inversions for pyrope are the TO–LO pairs computed at 139.8–138.7, 348.6–348.2, and 885.1–896.0 $cm^{-1}$ that produce LO–TO splittings of $-1.1$, $-0.4$, and $-10.9$ $cm^{-1}$, respectively. The tiny values computed for the two first pairs is due to the fact that diagonal elements of the $W^{NA}$ matrix (and then, to first order in the perturbation expansion, the LO–TO splitting) is proportional to the square of the dipole transition moment (or to the absorption strength as documented by Hofmesiter et al. and stated by Wooten[39]). Thus, moderate splitting is expected in general for weak intensities; on the contrary, larger splitting for the most intense TO modes. Some examples are the modes computed at 459.1 and 864.8 $cm^{-1}$, which have LO–TO splittings of 67.7 and 74.8 $cm^{-1}$, respectively.

LO modes involved in inversions for grossular and andradite are indicated in Figures 2 and 3, respectively. The analysis performed for pyrope also applies to these cases. Four LO–TO reversals are computed at 406.7–407.0, 480.1–480.8, 508.6–509.3, and 845.6–849.6 $cm^{-1}$ for grossular, whereas only three inversions at 313.7–313.8, 807.5–813.3, and 848.7–869.6 $cm^{-1}$ are identified for andradite.

## Conclusions

The Transverse Optical and Longitudinal Optical IR vibrational frequencies and intensities of pyrope, grossular, and andradite were calculated at the *ab initio* quantum mechanical level and compared with various sets of experimental data. The agreement with experimental results available is excellent. Because calculations provide the full set of frequencies, they permit one to complete the experimental set for frequencies not easily detectable experimentally, as those characterized by low intensity. The problem of the TO-LO splitting is discussed in its formal aspects, and with reference to the present cases. Excellent agreement with experiment was also observed concerning TO–LO splitting. The present study confirms that simulation is nowadays able to describe the structural and vibrational properties of large unit cell systems like garnets, and can then be used as a complementary tool to many experimental techniques.

## Acknowledgments

CINECA supercomputing center is acknowledged for allowance of computer time. F.J.T. acknowledges Regione Piemonte for his Ph.D. grant (Ab-initio simulation of the hydrogen storage in microporous materials).

## References

1. Deer, W.; Howie, R. Zussman, J. An Introduction to the Rock Forming Minerals, Wiley: New York, 1992.
2. Hofmeister, A. M.; Chopelas, A. Am Mineral 1991, 75, 880.
3. Hofmeister, A. M.; Chopelas, A. Phys Chem Minerals 1991, 17, 503.
4. Pascale, F.; Zicovich-Wilson, C. M.; Orlando, R.; Roetti, C.; Ugliengo, P.; Dovesi, R. J Phys Chem B 2005, 109, 6146.
5. Pascale, F.; Catti, M.; Damin, A.; Orlando, R.; Saunders, V. R.; Dovesi, R. J Phys Chem B 2005, 109, 18522.
6. Kolesov, B.; Geiger, C. A. Phys Chem Minerals 1998, 25, 142.
7. Kolesov, B.; Geiger, C. A. Phys Chem Minerals 2000, 27, 645.
8. McAloon, B. P.; Hofmeister, A. M. Am Mineral 1995, 80, 1145.
9. Bosenick, A.; Geiger, C. A.; Schaller, T.; Sebald, A. Am Mineral 1995, 80, 691.
10. Hofmeister, A. M.; Fagan, T. J.; Campbell, K. M.; Schaal, R. B. Am Mineral 1996, 81, 418.
11. Dovesi, R.; Saunders, V. R.; Roetti, C.; Orlando, R.; Zicovich-Wilson, C. M.; Pascale, F.; Doll, K.; Harrison, N. M.; Civalleri, B.; Bush, I. J.; D'Arco, P.; Llunell, M. Crystal06 User's Manual. Università di Torino, Torino, 2006.
12. Becke, A. D. J Chem Phys 1993, 98, 5648.
13. Koch, W.; Holthausen, M. C. A Chemist's Guide to Density Functional Theory; Wiley-VCH Verlag GmbH: Weinheim, 2000.
14. Zicovich-Wilson, C. M.; Pascale, F.; Roetti, C.; Saunders, V. R.; Orlando, R.; Dovesi, R. J Comput Chem 2004, 25, 1873.
15. Prencipe, M.; Pascale, F.; Zicovich-Wilson, C. M.; Saunders, V. R.; Orlando, R.; Dovesi, R. Phys Chem Minerals 2004, 31, 559.
16. Orlando, R.; Torres, F. J.; Pascale, F.; Ugliengo, P.; Zicovich-Wilson, C. M.; Dovesi, R. J Phys Chem B 2006, 110, 692.
17. Tosoni, S.; Pascale, F.; Ugliengo, P.; Orlando, R.; Saunders, V. R.; Dovesi, R. Mol Phys 2005, 103, 2549.
18. Available at: http://www.crystal.unito.it/supplement/garnets/garnets_inputs.tar.gz.
19. Pavese, A.; Artioli, G.; Prencipe, M. Am Mineral 1995, 80, 457.
20. Mittal, R.; Chaplot, S.; Choudhury, N. Phys Rev B 2001, 64, 094302.
21. Armbruster, T.; Geiger, C. A. Eur J Mineral 1993, 5, 59.
22. Pascale, F.; Zicovich-Wilson, C. M.; Gejo, F. L.; Civalleri, B.; Orlando, R.; Dovesi, R. J Comput Chem 2004, 25, 888.
23. Resta, R. J Phys Condens Matter, 2000, 12, R107.
24. Zicovich-Wilson, C. M.; Dovesi, R.; Saunders, V. R. J Chem Phys 2001, 115, 9708.
25. Baranek, P.; Zicovich-Wilson, C. M.; Roetti, C.; Orlando, R.; Dovesi, R. Phys Rev B 2001, 64, 125102.
26. Noel, Y.; Zicovich-Wilson, C. M.; Civalleri, B.; D'arco, P.; Dovesi, R. Phys Rev B 2002, 65, 014111.
27. Zicovich-Wilson, C. M.; Bert, A.; Roetti, C.; Dovesi, R.; Saunders, V. R. J Chem Phys 2002, 116, 1120.
28. Darrigan, C.; Rerat, M.; Mallia, G.; Dovesi, R. J Comput Chem 2003, 24, 1305.
29. Shannon, R.; Rossman, G. Am Mineral 1992, 77, 94.
30. Medenbach, O.; Shannon, R. D. J Opt Soc Am B 1997, 14, 3299.
31. Born, M.; Huang, K. Dynamical Theory of Crystal Lattices; Oxford University Press: Oxford, 1954.
32. Umari, P.; Pasquanello, A.; Corso, A. D. Phys Rev B 2001, 63, 094305.
33. Lax, M. Symmetry Principles in Solid State and Molecular Physics; Wiley: New York, 1974.
34. Ugliengo, P.; Viterbo, D.; Chiari, G. Z Kristallogr 1993, 207, 9.
35. Jmol's web site. Available at: http://jmol.sourceforge.net/.
36. Giesting, P. A.; Hofmeister, A. M. Phys Rev B 2002, 65, 144305.
37. Animation of garnet LO and TO vibration modes. Available at http://www.crystal.unito.it/prtfreq/jmol.html.
38. Chaplin, T.; Price, G. D.; Ross, N. L. Am Mineral 1998, 83, 841.
39. Wooten, F. Optical Properties of Solids; Academic Press: San Diego California, 1972.